

The effect of impregnation sequence on the hydrogenation activity and selectivity of supported Pt/Ni bimetallic catalysts

Yuying Shu ^{a,1}, Luis E. Murillo ^b, Jeffrey P. Bosco ^a, Wei Huang ^a,
Anatoly I. Frenkel ^c, Jingguang G. Chen ^{a,*}

^aDepartment of Chemical Engineering, Center for Catalytic Science and Technology, University of Delaware, Newark, DE, 19711, United States

^bDepartment of Materials Science and Engineering, Center for Catalytic Science and Technology, University of Delaware, Newark, DE, 19711, United States

^cDepartment of Physics, Yeshiva University, New York, NY, 10016, United States

Received 3 October 2007; received in revised form 10 January 2008; accepted 21 January 2008
Available online 31 January 2008

Abstract

The effect of impregnation sequence on the formation of Pt/Ni bimetallic nanoparticles supported on γ -Al₂O₃ was investigated for catalysts with Pt/Ni atomic ratios of 3/1 and 1/1. These bimetallic catalysts were prepared with a fixed Pt loading (5 wt.%) by incipient impregnation of one metal precursor and calcination, followed by the impregnation of the second metal precursor and a second calcinations step. The disproportionation activity of cyclohexene and the hydrogenation selectivity of acetylene in ethylene were used as probe reactions to compare the effect of the impregnation sequence. The bimetallic Pt/Ni catalysts showed significantly higher activity toward the disproportionation of cyclohexene than either Pt/ γ -Al₂O₃ or Ni/ γ -Al₂O₃. For catalysts with the Pt/Ni ratio of 3/1, the Pt-first catalyst, 1/3Ni-1Pt/ γ -Al₂O₃, showed higher activity than the Ni-first catalyst, 1Pt-1/3Ni/ γ -Al₂O₃. The effect of impregnation sequence was not as significant for catalysts with the Pt/Ni ratio of 1/1. In addition, kinetic analysis of the selective hydrogenation of acetylene in ethylene revealed an increase in the acetylene hydrogenation selectivity for 1/3Ni-1Pt/ γ -Al₂O₃ as compared to both 1Pt-1/3Ni/ γ -Al₂O₃ and monometallic 1Pt/ γ -Al₂O₃. Extended X-ray absorption fine structure (EXAFS) measurements of the Pt L_{III} edge indicated that Pt–Ni bimetallic bonds were formed in 1/3Ni-1Pt/ γ -Al₂O₃ but not in 1Pt-1/3Ni/ γ -Al₂O₃. The Pt–Ni bonds were formed for the 1/1 ratio catalysts with both impregnation sequences. Overall, our results indicate that, at low Ni loadings, the impregnation sequence has a significant effect on the formation of Pt–Ni bimetallic bonds, which in turn lead to different catalytic behavior for both the disproportionation of cyclohexene and the selective hydrogenation of acetylene in ethylene.

© 2008 Elsevier B.V. All rights reserved.

Keywords: Impregnation sequence; Pt/Ni bimetallic catalysts; Hydrogenation; Disproportionation; Cyclohexene; Acetylene; Ethylene

1. Introduction

Bimetallic catalysts have proven to be important materials for many catalytic applications [1–4] and are well known for exhibiting properties that are distinctly different from those of the corresponding monometallic catalysts [2,5]. Many investigations combining experimental studies and theoretical calculations have been performed with the goal of correlating electronic properties of bimetallic surfaces with reaction

pathways [6–16]. Some of the probe reactions of the novel activities of the bimetallic catalysts include the disproportionation and hydrogenation of hexene and cyclohexene [17–20], the adsorption and decomposition of ethylene [17,21], the selective hydrogenation of acetylene in the presence of ethylene [22], and the selective hydrogenation of acrolein toward its corresponding unsaturated alcohol (2-propenol) [23], among others.

More recently, it has been demonstrated that the structure of the bimetallic surfaces also plays a significant role in controlling their electronic and catalytic properties [6,8,11,12,17,21]. For example, our group has shown that for a Ni/Pt(1 1 1) bimetallic surface with a Ni coverage at one monolayer (ML), Ni atoms can reside either on the surface to produce a Ni-terminated

* Corresponding author.

E-mail address: jgchen@udel.edu (J.G. Chen).

¹ Present address: W. R. Grace, Columbia, MD, United States.

Ni–Pt(1 1 1) surface or in the subsurface region to form a Pt-terminated Pt–Ni–Pt(1 1 1) subsurface structure [12]. The ML Pt–Ni–Pt(1 1 1) structure is characterized by unique chemical properties that are distinctively different from Pt(1 1 1), Ni(1 1 1), or the surface Ni–Pt–Pt(1 1 1) structure [12,18,21,23–25]. In particular, the ML Pt–Ni–Pt(1 1 1) structure bonds more weakly to atomic hydrogen and alkenes as compared to Ni–Pt–Pt(1 1 1), Pt(1 1 1) and Ni(1 1 1) surfaces. Density function theory (DFT) modeling of these surfaces reveals that the modification of Pt(1 1 1) with subsurface Ni and other 3d transition metals at a monolayer coverage significantly alters the average energy of the surface Pt d-band (d-band center). Subsequent theoretical and experimental studies show that the ML Pt–Ni–Pt(1 1 1) structure is very active toward the hydrogenation of the C=C bonds [18,19,21]. Furthermore, this bimetallic structure is thermodynamically stable either in vacuum or with adsorbed atomic hydrogen [26], while the subsurface Ni atoms segregate to the surface in the presence of adsorbed oxygen [16]. The activation barrier for the transformation of the subsurface to surface structures is relatively low, ~ 15 kcal/mol, indicating that the segregation and diffusion of Ni atoms can potentially occur during calcination and reduction procedures and under reaction conditions.

The primary objectives of the current paper are two-fold. The first is to extend surface science studies of Pt/Ni bimetallic systems to supported bimetallic catalysts. The second objective is to determine the effect of impregnation sequence on the formation of bimetallic bonds. To achieve these objectives, we synthesized bimetallic catalysts with Pt/Ni atomic ratios of 3/1 and 1/1 by sequential impregnation with either Ni-first or Pt-first. The disproportionation of cyclohexene and the selective hydrogenation of acetylene in ethylene were chosen as probe reactions. The formation of the Pt–Ni bimetallic bond was investigated using EXAFS. Furthermore, the effect of impregnation sequences on the disproportionation activity of cyclohexene and hydrogenation selectivity of acetylene was investigated using Fourier transform infrared (FTIR) in a batch reactor.

Our group has previously used the disproportionation (self-hydrogenation) of cyclohexene as a probe reaction to compare the unique low-temperature hydrogenation activity of Pt/Ni bimetallic surfaces and catalysts. A low-temperature disproportionation pathway was detected on the Pt–Ni–Pt(1 1 1) subsurface structure prepared on Pt(1 1 1) [21] and on the Pt–Ni(1 1 1) surface structure prepared on Ni(1 1 1) [18], with both structures characterized by a Pt surface modified by Ni atoms underneath. In contrast, the disproportionation pathway did not occur on Pt(1 1 1), Ni(1 1 1), or the Ni–Pt–Pt(1 1 1) surface structure under the ultra-high vacuum (UHV) conditions. Because the disproportionation of cyclohexene is sensitive to whether the surface is terminated by Pt or Ni, it is chosen as one of the probe reactions in the current study to determine how the disproportionation activity is affected on Pt/Ni supported catalysts by the impregnation sequence. The second probe reaction is the selective hydrogenation of acetylene in ethylene, which is an important industrial process and has been the subject of many studies [27–35]. Previous studies showed that the formation of bimetallic alloys often

modifies the hydrogenation selectivity of acetylene, as demonstrated in the systematic investigations over Pd–Ag, Pd–Cu, and Pd–Au supported catalysts [36–38]. Therefore, the hydrogenation of acetylene should be a useful probe reaction to determine the effect of impregnation sequence on the hydrogenation selectivity of supported Pt/Ni catalysts.

2. Experimental

2.1. Materials

The γ -Al₂O₃ support (Alfa Aesar) was used as received. Pt(NH₃)₄(NO₃)₂ (Alfa Aesar) and Ni(NO₃)₂·6H₂O (Alfa Aesar, 99.9985%) were used as chemical precursors in the synthesis of the bimetallic catalysts. H₂ (Keen, grade 5), 10.0% acetylene/helium (Matheson, research grade), ethylene (Matheson, research grade) and CO (Matheson, research grade, 99.99%) were used as received. Cyclohexene (c-C₆H₁₀) (Aldrich, 99 + % purity) was purified using several freeze–pump–thaw cycles before use in the FTIR experiments.

2.2. Catalyst preparation

The γ -Al₂O₃ supported Pt/Ni bimetallic catalysts were prepared by sequential impregnation using the incipient wetness method at two Pt/Ni atomic ratios, 3/1 and 1/1, with the Pt loading being constant at 5 wt.%. The Ni loadings were 1.5 wt.% and 0.5 wt.%, respectively. The incipient wetness point of the dried γ -Al₂O₃ support was determined to be 0.75 cm³ g⁻¹. The Pt and Ni solutions were prepared by adding the necessary volume of deionized water to the metal precursor salts. After the impregnation of the first precursor (for Pt or Ni) the catalysts were dried at 383 K for 5 h followed by calcination in air at 563 K for 3 h before impregnating the second precursor (Ni or Pt). The resultant solid mixture was again dried and calcined in air following the aforementioned procedure.

For the remainder of this paper, the bimetallic samples are denoted as 1Ni-1Pt/ γ -Al₂O₃, 1Pt-1Ni/ γ -Al₂O₃, 1/3Ni-1Pt/ γ -Al₂O₃, and 1Pt-1/3Ni/ γ -Al₂O₃. The Ni-Pt/ γ -Al₂O₃ nomenclature means that Pt is impregnated first, while Pt-Ni/ γ -Al₂O₃ means that Ni is impregnated first. The 1Ni-1Pt notation represents 1:1 atomic ratio of Ni and Pt, which corresponds to a loading of ~ 1.5 wt.% and ~ 5 wt.%, respectively; the 1/3Ni-1Pt notation indicates that the atomic ratio of Ni-to-Pt is 1/3, corresponding to a Ni loading of ~ 0.5 wt.%.

2.3. Catalyst characterization

The metal dispersion of the catalysts was determined from carbon monoxide (CO) chemisorption experiments using an Altamira Instruments (AMI-200ip). A sample of 0.1 g was loaded into a quartz reactor and reduced in dilute hydrogen (50% H₂/He) at 723 K for 1 h. After cooling in He, pulses of CO in a He carrier gas at 20 cm³ min⁻¹ were injected at room temperature through a sample loop and the signal was monitored with a thermal conductivity detector (TCD). The CO uptake and metal dispersion were calculated by measuring

Table 1
CO uptake and metal dispersion from CO chemisorption measurements

Sample	CO uptake ($\mu\text{mol g}^{-1}$)	Dispersion (%)
1Pt/ γ -Al ₂ O ₃	71.9	28.1
1/3Ni-1Pt/ γ -Al ₂ O ₃	86.0	25.2
1Pt-1/3Ni/ γ -Al ₂ O ₃	83.6	24.5
1Ni-1Pt/ γ -Al ₂ O ₃	130.0	25.4
1Pt-1Ni/ γ -Al ₂ O ₃	122.3	23.9
1Ni/ γ -Al ₂ O ₃	37.0	14.5

the decrease in the peak areas caused by adsorption in comparison with the area of a calibrated volume (58 μmol), assuming a stoichiometry of one CO molecule per surface metal atom. The CO uptake and metal dispersion of the bimetallic Pt/Ni samples are shown in Table 1. The CO chemisorption results reveal that the dispersion is similar on the four bimetallic catalysts.

The catalyst samples were also characterized by high-angle annular dark-field scanning transmission electron microscopy (HAADF-STEM) using a JEOL 2010f electron microscope operating at 200 kV to determine the metal particle size on the support. The catalyst powders were sonicated in an ethanol solution for about 1 h. Immediately after sonication, two drops of the liquid were transferred onto a Lacey carbon support film on a copper grid. To make sure that the solvent was completely evaporated from the support, the TEM characterization was performed after 48 h of drying.

In order to detect the formation of Pt–Ni bimetallic bond, Pt L_{III}-edge EXAFS experiments were conducted on the X18B beamline at the National Synchrotron Light Source (NSLS), Brookhaven National Laboratory. Specimens were prepared by pressing a catalyst powder using hydraulic press (3 ton) to form self-supported pellets to be loaded into an in-house designed catalyst reactor that allowed one to collect X-ray fluorescence and transmission signals simultaneously over an operating temperature range of 150–773 K. The samples were heated under a diluted hydrogen flow (5% H₂ in He, 40 cc/min) to 723 K with a heating rate of 10 K min⁻¹. The catalysts were maintained at this temperature for 1 h and then cooled down under diluted H₂ flow. EXAFS data were collected at the L_{III} edge at room temperature using a double crystal Si(1 1 1) monochromator and ionization chambers. Reference Pt foil was measured in transmission mode simultaneously with all the samples for energy calibration.

The IFFEFIT 1.2.9 data analysis package (Athena, Artemis, Atoms and FEFF6) was used to analyze and fit the EXAFS data [39,40]. The reduction of the raw data was done by fitting the pre-edge region, aligning the individual scans, deglitching the scans in energy range if needed, normalizing to the edge jump, and then averaging to minimize the experimental errors. The AUTOBK algorithm was also used in Athena for background subtraction. Local structural information was obtained using Artemis [40] to fit each Pt-edge data set with theoretical standards generated from FEFF6 [41] in *r*-space. The Pt–Pt and Pt–Ni contributions to theoretical EXAFS were taken into account for the data fitting. The Pt–Pt FEFF theoretical

photoelectron amplitudes and phases were calculated for the bulk Pt fcc structure. The Pt–Ni contribution was calculated theoretically with FEFF6 by replacing Pt with Ni as the first nearest-neighbor shell to Pt in the Pt cluster. The variables in the fit were the coordination numbers of Pt–Ni and Pt–Pt bonds, corrections to their model distances and their disorders (σ^2 or Debye–Waller factors). The passive electron reduction factor, $S_0^2 = 0.87$, and the correction to the photoelectron energy origin were determined from the fits to the standard Pt foil EXAFS and fixed in the analysis of the supported catalysts. The total number of variables (7) was much smaller than the total number of the relevant independent data points (17).

2.4. FTIR studies

Fourier transform infrared spectroscopy was used to monitor the products and reaction kinetics of the disproportionation of cyclohexene and the selective hydrogenation of acetylene in the presence of ethylene using a batch reactor system. For all the FTIR experiments, catalyst pellets of ~ 40 mg were pressed onto a rectangular tungsten mesh (2.4 cm \times 1 cm, 100 mesh, 0.001 in wire diameter, Alfa Aesar), with spot-welded chromel–alumel thermocouple wires to monitor the temperature. The tungsten mesh was supported to a mounting bracket made of Nickel connected at the end of a Z-translator manipulator feedthrough. The feedthrough also possessed connections for resistive heating. The design of this type of cell was based on a model reported elsewhere [42]. The stainless steel IR cell, consisting of BaF₂ windows, allowed for in situ reduction of samples and spectroscopic measurements of surface species and gas-phase products. Spectra were recorded at room temperature with 4 cm⁻¹ spectral resolution by collecting 128 scans for gas phase using a Nicolet-510 FTIR spectrometer equipped with a MCT-A (mercury cadmium telluride) detector. To remove water and other impurities the cell was first evacuated to a pressure below 10⁻⁶ Torr for 60 min. The catalyst was then reduced at 723 K in 30 Torr hydrogen for 30 min followed by evacuation and a high-temperature flash (723 K) to remove any surface species generated during reduction. The reduction cycle was repeated three times before performing the FTIR experiments. The gases and vapors of liquid for reduction, venting, adsorption or hydrogenation reaction were admitted to the IR cell through a gas manifold.

For the disproportionation of cyclohexene, the gas-phase reaction products were monitored by recording gas-phase spectra every 30 s during the reaction. The purity of cyclohexene was verified in situ by comparing the IR spectrum with the standard reference reported in the literature [43]. The IR cell was initially filled with 9.8 Torr cyclohexene and gas-phase IR spectra were recorded at room temperature. For data analysis, the concentrations of the three main gas-phase species during the disproportionation reaction, cyclohexene, cyclohexane, and benzene, were estimated using the intensities of their vibrational modes at 1139 cm⁻¹ (ωCH_2 rock) [44], 1458 cm⁻¹ ($-\text{CH}_2$ deformation) [45], and 1810 cm⁻¹ (overtone of the C–C stretching mode at 993 cm⁻¹) [46], respectively. It is important to point out that the $-\text{CH}_2$ deformation mode at 1458 cm⁻¹ for

cyclohexane is convoluted with both the $-\text{CH}_2$ deformation feature at 1455 cm^{-1} for cyclohexene and the ring stretching and deformation feature at 1488 cm^{-1} for benzene. Therefore, contributions of the latter were subtracted when estimating the concentration of cyclohexane, as described previously [20]. These values were then normalized to the weight of catalyst used in the experiment.

Prior to performing the selective hydrogenation of acetylene in the presence of ethylene, a mixture of 10% acetylene in 90% helium (Matheson) was passed through a dry ice–acetone trap for its purification. During the hydrogenation of acetylene, the IR cell was filled with 10 Torr 10% acetylene and 1 Torr ethylene. After the equilibration of the reactant mixture and the formation of a stable baseline, 6 Torr of H_2 were introduced to initiate the reaction at room temperature and the IR spectra were recorded. The concentrations of the three main species, acetylene, ethylene, and ethane were determined by the classical least-squares method with a 16-member training set using the Beer–Lambert law [47] for the C–H stretching vibrational features between 2600 cm^{-1} and 3500 cm^{-1} , as described in detail previously [22].

A parametric fitting method was used for the hydrogenation of both acetylene and ethylene. Equilibrium constants K_1 , K_2 , and K_3 were defined for the adsorption of acetylene, ethylene and the dissociative adsorption of hydrogen. Also, k_1 and k_2 were defined as the rate constants for the hydrogenation of acetylene and ethylene, respectively. More details about the kinetic fitting of acetylene hydrogenation in the presence of ethylene have been described previously [22]. In brief, a Langmuir–Hinshelwood classical approximation was used for the elementary reactions that take place for the different reactants on the catalytic system. Rates of hydrogenation for acetylene and ethylene, as well as for the generation of ethane and consumption of hydrogen were used to derive the kinetic equations. The resultant equations were fitted with the experimental data to estimate the different constants [22].

3. Results and discussion

3.1. Particle distribution of Ni-Pt/ $\gamma\text{-Al}_2\text{O}_3$ and Pt-Ni/ $\gamma\text{-Al}_2\text{O}_3$ catalysts

Fig. 1 shows the HAADF-STEM pictures of Ni-Pt/ $\gamma\text{-Al}_2\text{O}_3$ and Pt-Ni/ $\gamma\text{-Al}_2\text{O}_3$ samples for Pt/Ni atomic ratios of 1/1 and 3/1. The samples were reduced in H_2 in the FTIR cell, although they were subsequently exposed to air during the sample preparation for TEM measurements. Since in the HAADF images the contrast arises due to difference in atomic number of the elements of interest (single heavy atoms on low- Z substrates) [48], the bright dots are most likely due to Pt and Ni particles distinguished from the low atomic number of the support ($\gamma\text{-Al}_2\text{O}_3$). The TEM images reveal a relatively uniform distribution of the metal particles (bright spots), with metal particle size in the range of $\sim 2\text{--}3\text{ nm}$, for all four catalysts. The similar particle size distributions are consistent with the similar dispersion values (Table 1) for the four Pt-Ni bimetallic catalysts.

3.2. EXAFS characterization of Ni-Pt/ $\gamma\text{-Al}_2\text{O}_3$ and Pt-Ni/ $\gamma\text{-Al}_2\text{O}_3$ catalysts

Fig. 2(a and b panels) shows the Pt- L_{III} -edge X-ray absorption near-edge structure (XANES) spectra of a Pt foil and of the 1/3Ni-1Pt/ $\gamma\text{-Al}_2\text{O}_3$ and 1Pt-1/3Ni/ $\gamma\text{-Al}_2\text{O}_3$ catalysts before and after reduction. The background-subtracted, edge step normalized and k^2 -weighted Pt L_{III} -edge EXAFS data ($\chi(k)$) are shown in r -space (Fig. 2c and d). Fourier transforms were performed using a k -range between 2 \AA^{-1} and 17 \AA^{-1} and the Hanning window function with sill width $\Delta k = 2\text{ \AA}^{-1}$.

Visual examination of the Pt L_{III} -edge XANES and EXAFS allows one to make the following preliminary conclusions about the state of reduction in each sample [49]. There is evidence of Pt–O and Pt–M (M = Pt and Ni) peaks in r -space in the Pt L_{III} -edge EXAFS (Fig. 2c and d) before reduction. The peak at low radial distribution, characteristic of Pt–O, in the unreduced sample is no longer present after reduction with hydrogen (Fig. 2c and d). These observations are consistent with the XANES results (Fig. 2a and b), which show that the white line intensity decreased toward that of Pt foil after the H_2 reduction.

Fig. 3 displays the Fourier transform of the experimental data after reduction with H_2 and the fit using FEFF6 [41] theory in r -space for 1/3Ni-1Pt/ $\gamma\text{-Al}_2\text{O}_3$, 1Pt-1/3Ni/ $\gamma\text{-Al}_2\text{O}_3$, 1Ni-1Pt/ $\gamma\text{-Al}_2\text{O}_3$, and 1Pt-1Ni/ $\gamma\text{-Al}_2\text{O}_3$. The best fit results are summarized in Table 2. The EXAFS spectra were analyzed by assuming two contributions, Pt–Pt and Pt–Ni. From the r -space, as explained above, Pt–O bonds do not contribute significantly in the reduced catalysts, and thus their theoretical contributions were not included in the model. For samples at a Pt/Ni ratio of 3/1, the calculated values for the total Pt–M coordination numbers indicate that the average diameter of the nanoparticles in both cases can be estimated as ca. 3 nm, assuming a hemispherical cuboctahedral fcc structure [50]. In addition, a small coordination of Pt–Ni is observed on the 1/3Ni-1Pt/ $\gamma\text{-Al}_2\text{O}_3$ while no Pt–Ni bonds were found on the 1Pt-1/3Ni/ $\gamma\text{-Al}_2\text{O}_3$ sample. On contrary, the results for the 1Ni-1Pt/ $\gamma\text{-Al}_2\text{O}_3$ and 1Pt-1Ni/ $\gamma\text{-Al}_2\text{O}_3$ samples confirmed the formation of Pt–Ni bonds in both impregnation sequences. For example, for the 1Pt-1Ni/ $\gamma\text{-Al}_2\text{O}_3$ sample, the Pt–Ni bond length was found to be $2.57(4)\text{ \AA}$, which is $0.07(4)\text{ \AA}$ longer than the Ni–Ni bond in metallic Ni (2.49 \AA) and $0.21(4)\text{ \AA}$ shorter than the Pt–Pt bond in metallic Pt (2.78 \AA). The Pt–Pt bond length is $2.74(1)\text{ \AA}$, which is $0.03(1)\text{ \AA}$ shorter than in metallic Pt (2.78 \AA). Both of these results suggest that Pt and Ni are in the alloy form. Furthermore, a good fit to the Pt L_{III} -edge data can only be obtained when both Pt–Pt and Pt–Ni contributions are included in the model, suggesting that the nanoparticles have both Pt and Ni.

In all four samples the ratio of the coordination numbers of Pt–Pt and Pt–Ni is greater than the atomic ratios of Pt/Ni. For example, in the two (1/1) catalysts the coordination number of Pt–Pt is greater than that of Pt–Ni, suggesting that the remaining Ni atoms are in the monometallic Ni phases either in particles or in dispersed form on the Al_2O_3 surface. Due to the relatively low loadings of Ni in these samples, the quality of the

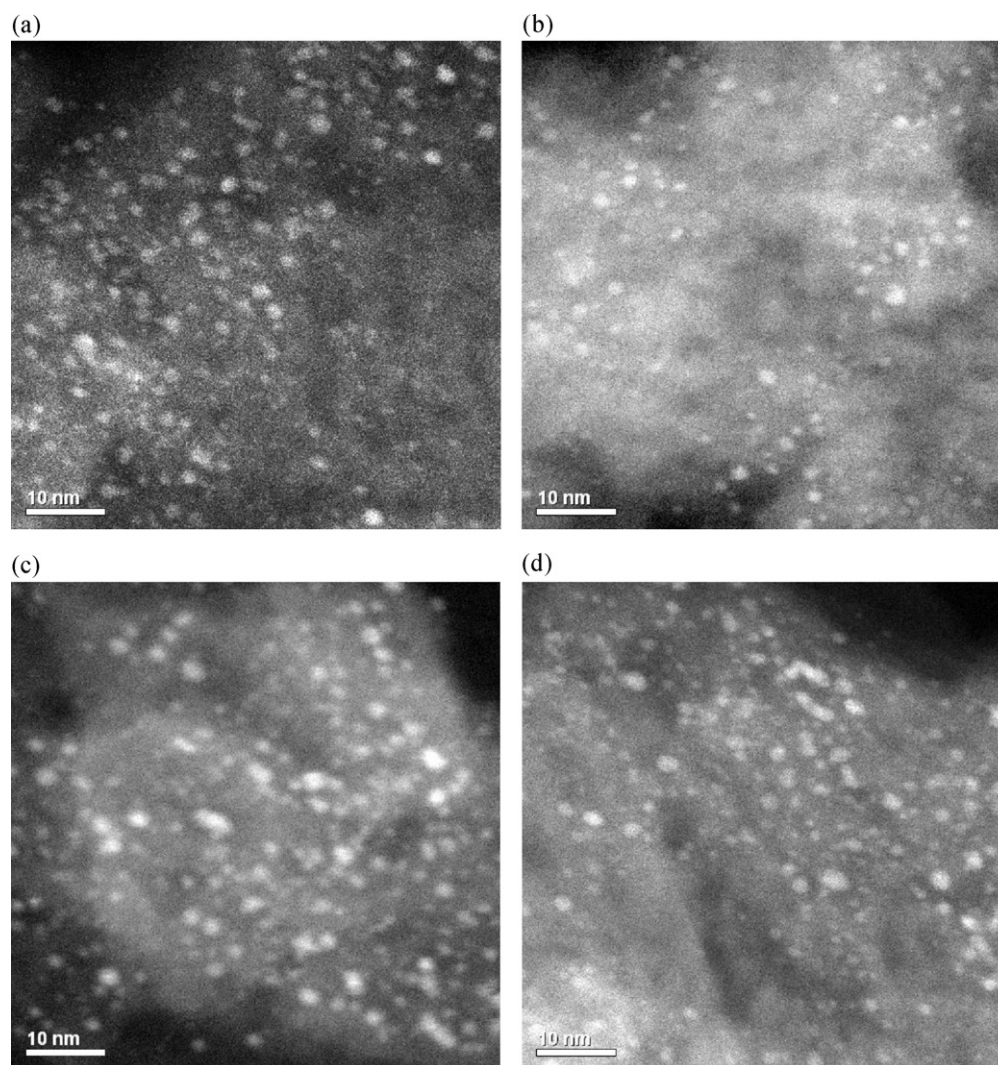


Fig. 1. TEM images of the samples: (a) 1/3Ni-1Pt/ γ -Al₂O₃, (b) 1Pt-1/3Ni/ γ -Al₂O₃, (c) 1Ni-1Pt/ γ -Al₂O₃, and (d) 1Pt-1Ni/ γ -Al₂O₃.

EXAFS spectra of the Ni K-edge was not sufficient for EXAFS analysis in the current study.

3.3. Activity of disproportionation of cyclohexene

Fig. 4a shows the rates of cyclohexene consumption, in units of number of molecules per mg of catalyst over the various Pt/Ni bimetallic catalysts and the corresponding monometallic catalysts for the disproportionation of cyclohexene. Fig. 4b and c displays the reaction products from the disproportionation, cyclohexene and benzene, respectively. As shown in Fig. 4a, for the 1Ni-1Pt/ γ -Al₂O₃ and 1Pt-1Ni/ γ -Al₂O₃ catalysts, the conversion of cyclohexene reached 100% after ~60 min. In contrast, the monometallic Pt and Ni catalysts showed significantly lower rates for the conversion of cyclohexene. The conversion of cyclohexene on the 1/3Ni-1Pt/ γ -Al₂O₃ catalyst was significantly faster than the one on 1Pt-1/3Ni/ γ -Al₂O₃. In order to obtain a more quantitative comparison, the conversion rate of cyclohexene on all the catalysts was approximated by fitting the experimental results with first-order kinetics. These rate constants are listed in Table 3. The rate constants for cyclohexene

conversion over the six catalysts followed the order of 1Pt/ γ -Al₂O₃ < 1Ni/ γ -Al₂O₃ < 1Pt-1/3Ni/ γ -Al₂O₃ < 1/3Ni-1Pt/ γ -Al₂O₃ < 1Pt-1Ni/ γ -Al₂O₃ \approx 1Ni-1Pt/ γ -Al₂O₃. The 1/3Ni-1Pt/ γ -Al₂O₃ catalyst clearly showed a higher disproportionation rate than 1Pt-1/3Ni/ γ -Al₂O₃. This can be explained by the presence of the Pt–Ni bimetallic alloy when Pt was impregnated first, as confirmed by the detection of the Pt–Ni bond from the EXAFS measurements. On the contrary, similar disproportionation rates were observed on both 1Ni-1Pt/ γ -Al₂O₃ and 1Pt-1Ni/ γ -Al₂O₃ catalysts, which means that the bimetallic effect on these Pt/Ni bimetallic catalysts does not depend strongly on the sequence in the impregnation of the metal precursors at the Ni metal loading used in these catalysts (1.5 wt.% Ni). Again this is consistent with the EXAFS results, where the presence of the Pt–Ni bonds is observed in both catalysts.

3.4. Hydrogenation selectivity of acetylene in the presence of ethylene

Fig. 5 compares the concentrations of gas-phase acetylene (C₂H₂), ethylene (C₂H₄), and C₂H₆ (ethane) as a function of

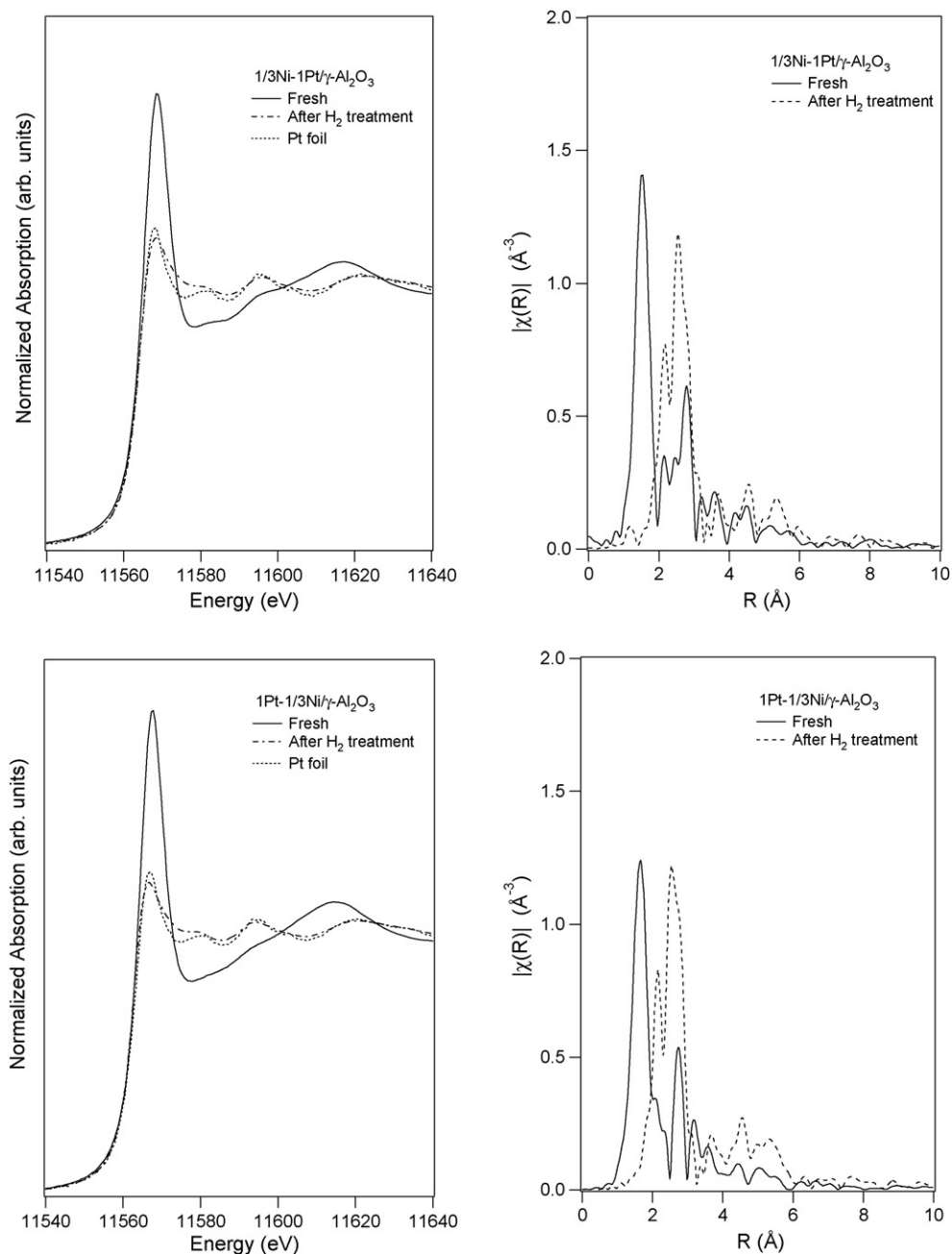


Fig. 2. Pt L_{III} -edge XANES spectra and EXAFS fit of 1/3Ni-1Pt/ γ - Al_2O_3 and 1Pt-1/3Ni/ γ - Al_2O_3 before reduction and after reduction.

reaction time over 1Ni/ γ - Al_2O_3 , 1Pt/ γ - Al_2O_3 , 1/3Ni-1Pt/ γ - Al_2O_3 , and 1Pt-1/3Ni/ γ - Al_2O_3 at room temperature. On the 1Pt/ γ - Al_2O_3 , 1/3Ni-1Pt/ γ - Al_2O_3 , and 1Pt-1/3Ni/ γ - Al_2O_3 catalysts, the acetylene concentration decreased during the reaction while ethane concentration increased until all the acetylene and ethylene were consumed. Due to presence of excess H_2 , the final product of all reactions was ethane. In contrast, the reaction over 1Ni/ γ - Al_2O_3 showed significantly lower hydrogenation activity, as shown in Fig. 5. It is apparent that different trends are observed over the different catalysts in the concentration profiles of acetylene, ethylene, and ethane. For example, the ethylene concentration went up noticeably for 1/3Ni-1Pt/ γ - Al_2O_3 while it decreased or remained practically

constant for 1Pt-1/3Ni/ γ - Al_2O_3 and 1Pt/ γ - Al_2O_3 catalysts from the very beginning of the reaction.

The fitted curves are shown in Fig. 6 and the estimated rate and equilibrium values based on surface active sites are summarized in Table 4. The kinetic equations used for the fitting were described previously for Pd-based bimetallic catalysts [22]. The hydrogenation selectivity of acetylene on the 1/3Ni-1Pt/ γ - Al_2O_3 catalyst was higher than that on the 1Pt-1/3Ni/ γ - Al_2O_3 and 1Pt/ γ - Al_2O_3 catalysts. The selectivity on the 1Ni/ γ - Al_2O_3 catalyst was not determined due to the very low hydrogenation activity observed on this surface.

As shown in Table 4, on the 1/3Ni-1Pt/ γ - Al_2O_3 catalyst, the equilibrium constant for acetylene adsorption (K_1) is larger than

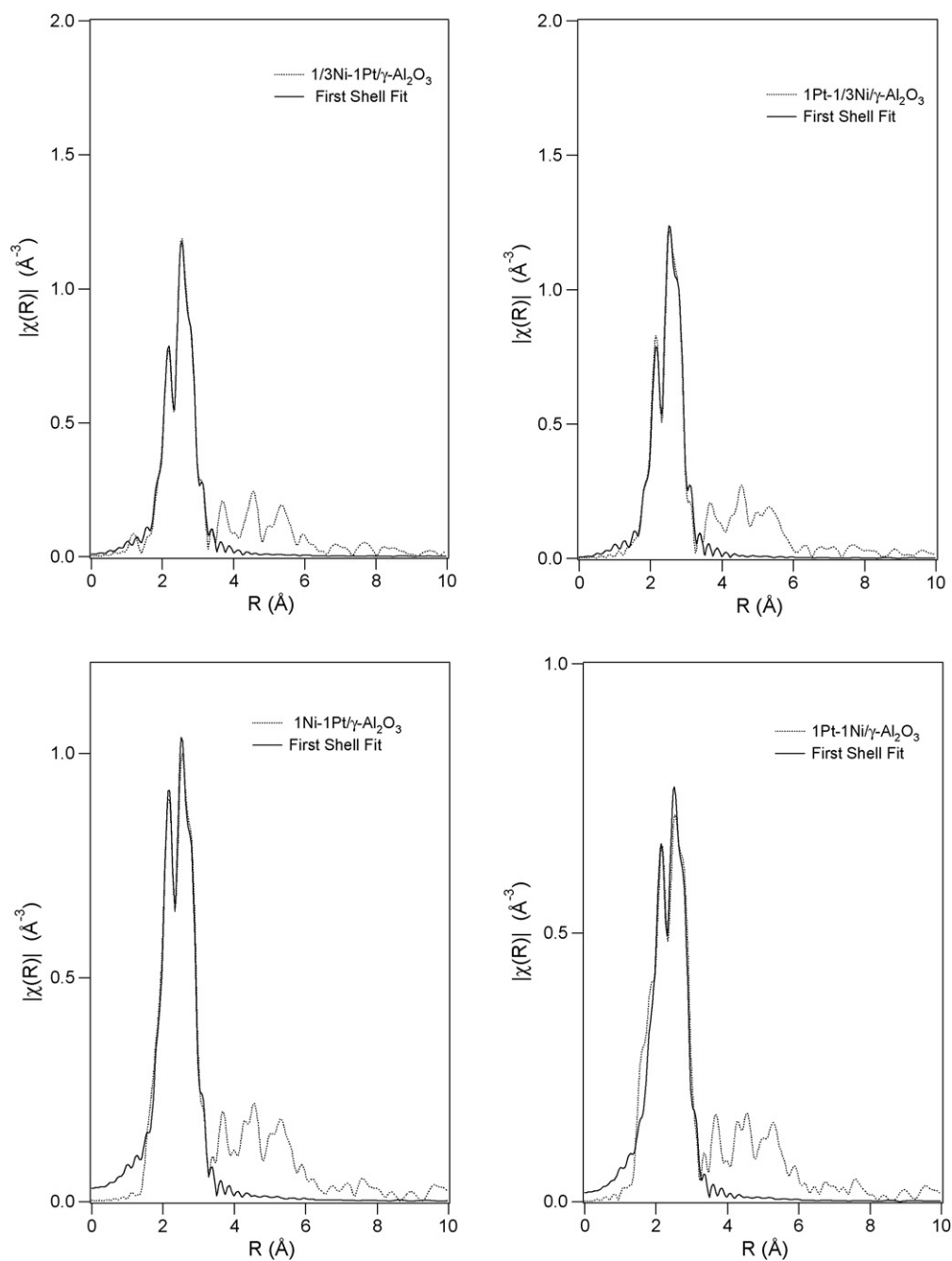


Fig. 3. Fourier-transformed (magnitude) k^2 -weighted EXAFS function ($\chi(k)$) of Pt L_{III} edge of 1/3Ni-1Pt/ γ -Al₂O₃, 1Pt-1/3Ni/ γ -Al₂O₃, 1Ni-1Pt/ γ -Al₂O₃, and 1Pt-1Ni/ γ -Al₂O₃, data (dashed) and fitted (solid) EXAFS curves.

Table 2

Results of Pt L_{III} -edge EXAFS fitting on 1/3Ni-1Pt/ γ -Al₂O₃, 1Pt-1/3Ni/ γ -Al₂O₃, 1Ni-1Pt/ γ -Al₂O₃, and 1Pt-1Ni/ γ -Al₂O₃

Sample	1/3Ni-1Pt/ γ -Al ₂ O ₃	1Pt-1/3Ni/ γ -Al ₂ O ₃	1Ni-1Pt/ γ -Al ₂ O ₃	1Pt-1Ni/ γ -Al ₂ O ₃
N(Pt–Pt)	8.0 ± 0.6	9.0 ± 0.4	8.2 ± 1.0	6.6 ± 1.6
N(Pt–Ni)	0.8 ± 0.6	0	2.6 ± 1.1	4.1 ± 3.3
R(Pt–Pt) (Å)	2.746 ± 0.002	2.75 ± 0.002	2.744 ± 0.003	2.739 ± 0.008
R(Pt–Ni) (Å)	2.60 ± 0.03	–	2.58 ± 0.02	2.572 ± 0.04
σ^2 (Pt–Pt) (Å ²)	0.0065 ± 0.0003	0.0064 ± 0.0002	0.0072 ± 0.0005	0.0076 ± 0.0011
σ^2 (Pt–Ni) (Å ²)	0.013 ± 0.0066	–	0.0141 ± 0.0036	0.022 ± 0.009

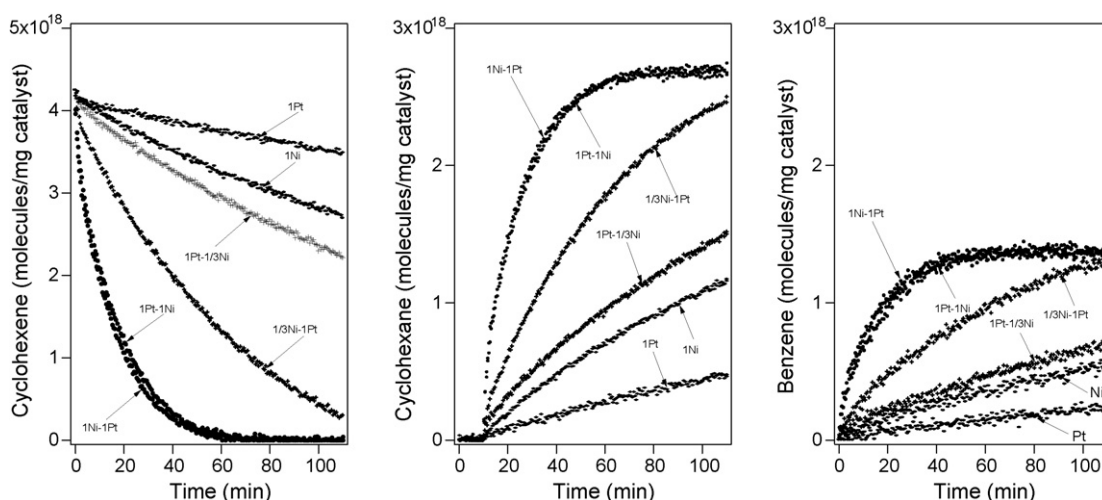


Fig. 4. Comparison of the rates of cyclohexene consumption and cyclohexane and benzene production over 1Pt/ γ -Al₂O₃, 1Ni/ γ -Al₂O₃, 1/3Ni-1Pt/ γ -Al₂O₃, 1Pt-1/3Ni/ γ -Al₂O₃, 1Ni-1Pt/ γ -Al₂O₃, and 1Pt-1Ni/ γ -Al₂O₃ catalysts at room temperature.

that on 1Pt-1/3Ni/ γ -Al₂O₃ or 1Pt/ γ -Al₂O₃, while the equilibrium constant for ethylene adsorption (K_2) is smaller than on the other catalysts. Therefore, the increase in the selectivity to acetylene hydrogenation on 1/3Ni-1Pt/ γ -Al₂O₃ is mainly due to the increase in the relative ratio of K_1/K_2 , which means alloying Pt with Ni can help adsorb more acetylene and less ethylene and thus lead to the enhancement of acetylene hydrogenation selectivity. The comparison indicates that hydrogenation selectivity of acetylene depends on the order at which the metal precursors are impregnated on the support.

3.5. Effect of impregnation sequence on the formation of bimetallic Pt–Ni bonds

In the case of the two 1/1 ratio catalysts, there is no significant difference between them in the overall activity for the disproportionation of cyclohexene and the estimated rate constants. Although the EXAFS analysis shows differences in the coordination number of the Pt–Ni bonds, the fact that Pt–Pt and Pt–Ni distances are very similar within the error bars implies that bimetallic bonds are formed on both catalysts. As mentioned in the introduction, the Pt-terminated bimetallic surfaces are much more active than Ni-terminated ones for the disproportionation cyclohexene [18]. Therefore, the observation of similar disproportionation activities of the 1Ni-1Pt/ γ -Al₂O₃ and 1Pt-1Ni/ γ -Al₂O₃ suggests that the surfaces of both catalysts are likely terminated by Pt after the calcination and reduction cycles. The segregation of Pt atoms to the surface is

consistent with previous studies on the Ni/Pt(1 1 1) surfaces, where the segregation of Pt is thermodynamically favored under ultra-high vacuum conditions and in the presence of atomic hydrogen [16]. Lastly, a similar finding has been reported for Ni/Pt catalysts supported on alumina for the reforming of methane. The authors concluded that the sequential impregnation of previously reduced Ni catalysts with Pt shows Pt atoms located preferentially on the surface of the Pt–Ni alloy [55].

In comparison, the physical and chemical probes described above demonstrate that the impregnation sequence has a significant effect on the formation of the Pt–Ni bimetallic bonds for catalysts with low Ni loading (~ 0.5 wt.% Ni), while the effect is much less for the catalysts with higher Ni loading (~ 1.5 wt.% Ni). With a Pt/Ni ratio of 3/1 (~ 0.5 wt.% Ni), the formation of the Pt–Ni bimetallic nanoparticles is evident when Pt is impregnated first on the alumina support, 1/3Ni-1Pt/ γ -Al₂O₃, as confirmed by the detection of the Pt–Ni coordination in EXAFS (See Table 2). In contrast, there is no evidence of bimetallic bond formation when the Ni precursor is impregnated first, 1Pt-1/3Ni/ γ -Al₂O₃. In addition, the disproportionation of cyclohexene on 1/3Ni-1Pt/ γ -Al₂O₃ shows a higher conversion rate than either 1Pt-1/3Ni/ γ -Al₂O₃ or 1Pt/ γ -Al₂O₃. Finally, the 1/3Ni-1Pt/ γ -Al₂O₃ catalyst also shows a higher selectivity for the hydrogenation of acetylene in the presence of ethylene than either 1Pt-1/3Ni/ γ -Al₂O₃ or 1Pt/ γ -Al₂O₃. All of these results suggest the lack of the formation of the bimetallic Pt–Ni bonds on the 1Pt-1/3Ni/ γ -Al₂O₃ catalyst. This could be due to the formation of Ni aluminate (NiAl₂O₄) species when Ni is impregnated first on the alumina support, due to the strong interaction of Ni with γ -Al₂O₃ as reported previously [51,52]. According to Morikawa et al. [53] and Salagre et al. [54], Ni in NiAl₂O₄ is reducible only at temperatures above 873 K, which is higher than the reduction temperature of 723 K in the current study. In comparison, for a higher Ni loading (1.5 wt.%) with a Pt/Ni ratio of 1/1 (5 wt.% Pt), bimetallic Pt–Ni bonds are detected regardless of the impregnation sequence, suggesting that there is a threshold of Ni loading for the formation of the

Table 3
Rate constants for cyclohexene conversion

Catalysts	k (s ⁻¹)
1Pt/ γ -Al ₂ O ₃	2.9×10^{-5}
1/3Ni-1Pt/ γ -Al ₂ O ₃	3.3×10^{-4}
1Pt-1/3Ni/ γ -Al ₂ O ₃	1.1×10^{-4}
1Ni-1Pt/ γ -Al ₂ O ₃	1.2×10^{-3}
1Pt-1Ni/ γ -Al ₂ O ₃	1.1×10^{-3}
1Ni/ γ -Al ₂ O ₃	7.2×10^{-5}

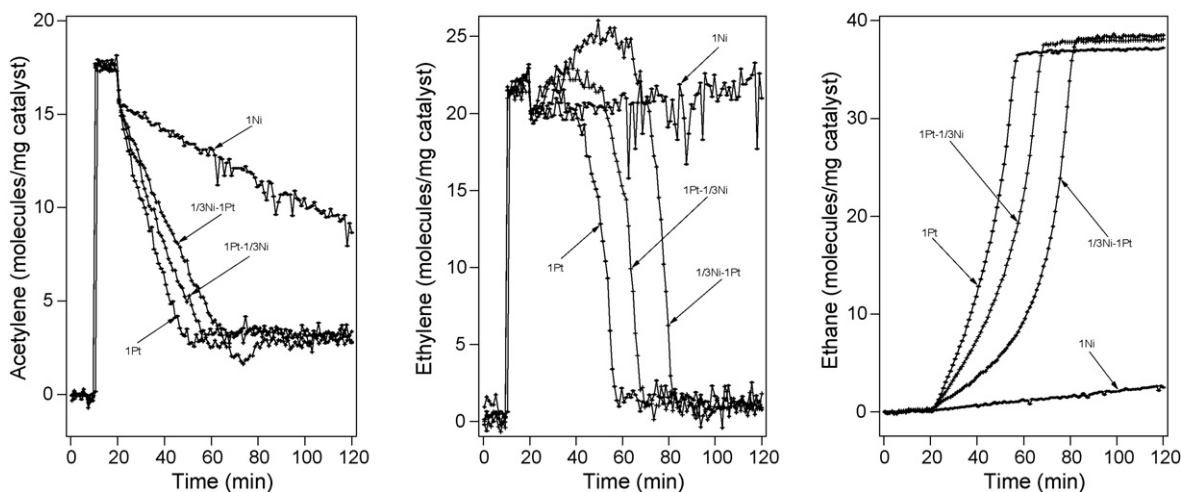


Fig. 5. Concentrations of gas-phase C_2H_2 , C_2H_4 , and C_2H_6 vs. reaction time at room temperature over 1Pt/ γ - Al_2O_3 , 1/3Ni-1Pt/ γ - Al_2O_3 , 1Pt-1/3Ni/ γ - Al_2O_3 , and 1Ni/ γ - Al_2O_3 .

Pt–Ni bimetallic bonds. It is most likely that an initial threshold coverage of Ni interacts strongly with the support, producing either NiO or $NiAl_2O_4$ that prevents the reduction of Ni and therefore the formation of the Pt–Ni bimetallic bonds. When Pt is impregnated first, the strong interaction of Ni with the support seems to be reduced by the Pt precursor or the actual Pt oxide formed during the calcination step. This could explain the fact that the 1/3Ni-1Pt/ γ - Al_2O_3 catalyst shows the presence of the Pt–Ni bonds, and correspondingly an enhanced selectivity in the hydrogenation of acetylene and a higher disproportionation activity of cyclohexene than 1Pt-1/3Ni/ γ - Al_2O_3 or 1Pt/ γ - Al_2O_3 .

Another explanation for the effect of impregnation sequence is the possible diffusion of Ni^{2+} ion into the tetrahedral and octahedral cavities of the γ - Al_2O_3 support. The ability of transition metal ions to enter the γ - Al_2O_3 lattice cavities should depend on the size of the ions. As reported by Yan et al. [56,57], small ions such as Ni^{2+} or Co^{2+} with a radius of 0.69 Å are well

known to enter the γ - Al_2O_3 matrix relatively easily, but the larger Pt^{2+} ion with a radius of 0.80 Å is unable to do so under the same conditions. The same argument could be applied in the current study. When the Ni^{2+} ion is impregnated first, all or a large fraction would enter the γ - Al_2O_3 cavities. On the contrary, if the Pt^{2+} is deposited first, it would remain outside the matrix and likely prevent subsequently deposited Ni^{2+} ion from entering the γ - Al_2O_3 cavities. The availability of both Ni and Pt outside the cavities would in turn facilitate the formation of the Pt–Ni bimetallic bonds, consistent with the results in the current study.

Overall, results from the reactors studies suggested that the catalytic properties of 1Pt-1/3Ni/ γ - Al_2O_3 catalyst were also modified as compared to the monometallic catalysts. This is indicated by the increase in the rate constant for cyclohexene conversion (Table 3) and in the equilibrium constant for acetylene adsorption (Table 4). Even though the modifications in these constants are less than those of the 1/3Ni-1Pt/ γ - Al_2O_3

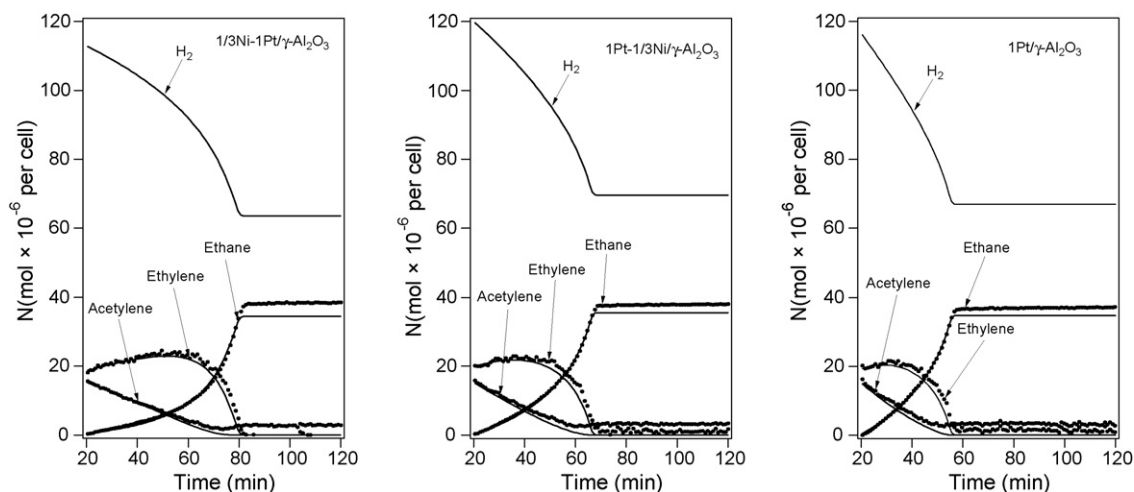


Fig. 6. Fitted concentrations of gas-phase C_2H_2 , C_2H_4 , and C_2H_6 vs. reaction time at room temperature over (a) 1/3Ni-1Pt/ γ - Al_2O_3 , (b) 1Pt-1/3Ni/ γ - Al_2O_3 , and (c) 1Pt/ γ - Al_2O_3 .

Table 4
Fitted values of rate and equilibrium constants and calculated values of selectivity

Catalysts	k_1	k_2	K_1	K_2	$S = (k_1/k_2) \times (K_1/K_2)$
1Pt/ γ -Al ₂ O ₃	5.6 ± 1.2	4.6 ± 0.1	9.6 ± 3.3	4.6 ± 0.1	2.4
1/3Ni-1Pt/ γ -Al ₂ O ₃	2.6 ± 0.2	3.2 ± 0.1	15.4 ± 1.1	3.1 ± 0.1	4.1
1Pt-1/3Ni/ γ -Al ₂ O ₃	3.5 ± 0.3	3.4 ± 0.2	13.6 ± 0.5	5.1 ± 0.8	2.8
1Ni/ γ -Al ₂ O ₃	–	–	–	–	–

catalyst, they nevertheless suggested that at least a fraction of the Pt and Ni atoms formed bimetallic bonds. Although the EXAFS analysis did not detect the Ni–Pt bonds in the 1Pt-1/3Ni/ γ -Al₂O₃ catalyst, this could be partially due to the sensitivity limit of EXAFS for the low loading of Ni.

4. Conclusions

From the results and discussion presented above, the following conclusions can be made regarding the effect of impregnation sequence on the physical and chemical properties of supported Pt–Ni bimetallic catalysts:

The impregnation sequence of Pt and Ni has a significant effect on the formation of Pt–Ni bimetallic bonds on the γ -Al₂O₃ support for a Pt/Ni atomic ratio of 3/1 (5 wt.% Pt, 0.5 wt.% Ni). When Pt is impregnated first, a significantly higher activity for the disproportionation of cyclohexene and a higher selectivity for the acetylene hydrogenation were found when compared with the one where Ni is impregnated first, 1Pt-1/3Ni/ γ -Al₂O₃. EXAFS measurements and data analysis show the formation of Pt–Ni bimetallic bonds on the former but not on the latter catalyst. One possible explanation of the effect of impregnation sequence is the diffusion of Ni into the cavities of the γ -Al₂O₃ support when the Ni²⁺ ion is deposited first.

For a higher Ni loading at the same Pt loading (1.5 wt.% Ni) in the bimetallic catalysts, the sequence of the impregnation does not seem to play a significant role in the catalytic activity for the disproportionation of cyclohexene. EXAFS studies reveal the formation of Pt–Ni bonds in both catalysts. The observation of similar disproportionation activities suggests that the surfaces of both are Pt-terminated, from the segregation of Pt to the surface during hydrogen reduction that has been predicted from DFT modeling verified experimentally in previous studies on single crystal Ni/Pt(1 1 1) surfaces [16].

Overall, the batch reactor results demonstrate that the bimetallic catalysts show higher hydrogenation activity and selectivity than the monometallic Pt and Ni catalysts. The promoting effect due to bimetallic formation is consistent with previous studies on the corresponding single crystal surfaces, demonstrating a correlation of Ni/Pt(1 1 1) and Pt/Ni(1 1 1) model surfaces with supported Pt/Ni bimetallic catalysts.

Acknowledgements

We acknowledge the financial support from the Department of Energy, Office of Basic Energy Sciences (Grant# DE-FG02-00ER15014). Use of the National Synchrotron Light Source, Brookhaven National Laboratory, for our EXAFS experiments

was supported by the U.S. Department of Energy, Office of Basic Energy Sciences (Grant# DE-FG02-05ER15688).

References

- [1] J.H. Sinfelt, *Acc. Chem. Res.* 10 (1977) 15–20.
- [2] J.H. Sinfelt, *Bimetallic Catalysts: Discoveries, Concepts, and Applications*, John Wiley & Sons, New York, 1983.
- [3] N.M. Markovic, P.N. Ross, *Electrochim. Acta* 45 (2000) 4101–4115.
- [4] N. Tsubaki, S.L. Sun, K. Fujimoto, *J. Catal.* 199 (2001) 236–246.
- [5] J.A. Rodriguez, *Surf. Sci. Rep.* 24 (1996) 225–287.
- [6] B. Hammer, J.K. Nørskov, *Surf. Sci.* 343 (1995) 211–220.
- [7] D.W. Goodman, *J. Phys. Chem.* 100 (1996) 13090–13102.
- [8] B. Hammer, J.K. Nørskov, *Adv. Catal.* 45 (2000) 71–129.
- [9] N.M. Markovic, P.N. Ross, *Surf. Sci. Rep.* 45 (2002) 121–229.
- [10] Y. Xu, A.V. Ruban, M. Mavrikakis, *J. Am. Chem. Soc.* 126 (2004) 4717–4725.
- [11] J. Greeley, M. Mavrikakis, *Nat. Mater.* 3 (2004) 810–815.
- [12] J.R. Kitchin, N.A. Khan, M.A. Barteau, J.G. Chen, B. Yakshinskiy, T.E. Madey, *Surf. Sci.* 544 (2003) 295–308.
- [13] J.R. Kitchin, J.K. Nørskov, M.A. Barteau, J.G. Chen, *J. Chem. Phys.* 120 (2004) 10240–10246.
- [14] J.R. Kitchin, J.K. Nørskov, M.A. Barteau, J.G. Chen, *Phys. Rev. Lett.* 93 (2004).
- [15] A.M. Goda, M.A. Barteau, J.G. Chen, *J. Phys. Chem. B* 110 (2006) 11823–11831.
- [16] C.A. Menning, H.H. Hwu, J.G. Chen, *J. Phys. Chem. B* 110 (2006) 15471–15477.
- [17] N.A. Khan, L.E. Murillo, J.G. Chen, *J. Phys. Chem. B* 108 (2004) 15748–15754.
- [18] N.A. Khan, M.B. Zellner, L.E. Murillo, J.G. Chen, *Catal. Lett.* 95 (2004) 1–6.
- [19] L.E. Murillo, N.A. Khan, J.G. Chen, *Surf. Sci.* 594 (2005) 27–42.
- [20] N.A. Khan, L.E. Murillo, Y.Y. Shu, J.G. Chen, *Catal. Lett.* 105 (2005) 233–238.
- [21] H.H. Hwu, J. Eng Jr., J.G. Chen, *J. Am. Chem. Soc.* 124 (2002) 702–709.
- [22] W. Huang, J.R. McCormick, R.F. Lobo, J.G. Chen, *J. Catal.* 246 (2007) 40–51.
- [23] L.E. Murillo, A.M. Goda, J.G. Chen, *J. Am. Chem. Soc.* 129 (2007) 7101–7105.
- [24] N.A. Khan, H.H. Hwu, J.G. Chen, *J. Catal.* 205 (2002) 259–265.
- [25] L.E. Murillo, J.G. Chen, *Surf. Sci.* 602 (2008) 919–931.
- [26] C.A. Menning, J.G. Chen, in preparation.
- [27] M.L. Derrien, *Stud. Surf. Sci. Catal.* 27 (1986) 613–666.
- [28] A. Molnar, A. Sarkany, M. Varga, *J. Mol. Catal. A-Chem.* 173 (2001) 185–221.
- [29] N.S. Schbib, M.A. Garcia, C.E. Gigola, A.F. Errazu, *Ind. Eng. Chem. Res.* 35 (1996) 1496–1505.
- [30] H. Nakatsuji, M. Hada, T. Yonezawa, *Surf. Sci.* 185 (1987) 319–342.
- [31] J.W. Medlin, M.D. Allendorf, *J. Phys. Chem. B* 107 (2003) 217–223.
- [32] P.A. Sheth, M. Neurock, C.M. Smith, *J. Phys. Chem. B* 107 (2003) 2009–2017.
- [33] S.G. Podkolzin, R. Alcalá, J.A. Dumesic, *J. Mol. Catal. A-Chem.* 218 (2004) 217–227.
- [34] J. Horiiuchi, M. Polanyi, *T. Faraday Soc.* 30 (1934) 1164–1172.

- [35] R.D. Cortright, S.A. Goddard, J.E. Rekoske, J.A. Dumesic, *J. Catal.* 127 (1991) 342–353.
- [36] L. Guzzi, Z. Schay, G. Stefler, L.F. Liotta, G. Deganello, A.M. Venezia, *J. Catal.* 182 (1999) 456–462.
- [37] A. Sarkany, A. Horvath, A. Beck, *Appl. Catal. A-Gen.* 229 (2002) 117–125.
- [38] P.A. Sheth, M. Neurock, C.M. Smith, *J. Phys. Chem. B* 109 (2005) 12449–12466.
- [39] M. Newville, *J. Synchrotron. Radiat.* 8 (2001) 96–100.
- [40] B. Ravel, M. Newville, *J. Synchrotron. Radiat.* 12 (2005) 537–541.
- [41] J.J. Rehr, R.C. Albers, *Rev. Mod. Phys.* 72 (2000) 621–654.
- [42] P. Basu, T.H. Ballinger, J.T. Yates, *Rev. Sci. Instrum.* 59 (1988) 1321–1327.
- [43] NIST, *Chemistry WebBook*.
- [44] A.V. Kiselev, V.I. Lygin, *Infrared Spectra of Surface Compounds*, John Wiley and Sons, New York, 1975.
- [45] T. Shimanouchi, *Tables of Molecular Vibrational Frequencies Consolidated*, National Bureau of Standards, 1972.
- [46] N.B. Colthup, L.H. Daly, S.E. Wiberley, *Introduction to Infrared and Raman Spectroscopy*, Academic Press, Inc., San Diego, 1990.
- [47] R. Kramer, *Chemometric Techniques for Quantitative Analysis*, CRC Press, New York, 1998.
- [48] D.B. Williams, C.B. Carter, *Transmission Electron Microscopy*, Plenum Press, New York, 1996.
- [49] A. Jentys, B.J. McHugh, G.L. Haller, J.A. Lercher, *J. Phys. Chem.* 96 (1992) 1324–1328.
- [50] A.I. Frenkel, C.W. Hills, R.G. Nuzzo, *J. Phys. Chem. B* 105 (2001) 12689–12703.
- [51] Y.G. Chen, J. Ren, *Catal. Lett.* 29 (1994) 39–48.
- [52] Z. Xu, Y.M. Li, J.Y. Zhang, L. Chang, R.Q. Zhou, Z.T. Duan, *Appl. Catal. A* 213 (2001) 65–71.
- [53] K. Morikawa, T. Shirasaki, M. Okada, *Adv. Catal.* 20 (1969) 97.
- [54] P. Salagre, J.L.G. Fierro, F. Medina, J.E. Sueiras, *J. Mol. Catal. A* 106 (1996) 125–134.
- [55] B.T. Li, S. Kado, Y. Mukainakano, T. Miyazawa, T. Miyao, S. Naito, K. Okumura, K. Kunimori, K. Tomishige, *J. Catal.* 245 (2007) 144–155.
- [56] J.Y. Yan, M.C. Kung, W.M.H. Sachtler, H.H. Kung, *J. Catal.* 172 (1997) 178–186.
- [57] J.Y. Yan, H.H. Kung, W.M.H. Sachtler, M.C. Kung, *J. Catal.* 175 (1998) 294–301.